Journal of the European Ceramic Society 22 (2002) 1947–1958

www.elsevier.com/locate/jeurceramsoc

Correlation between hydration mechanism and ultrasonic measurements in an aluminous cement: effect of setting time and temperature on the early hydration

A. Smith, T. Chotard*, N. Gimet-Breart, D. Fargeot

Groupe d'Etude des Matériaux Hétérogènes (GEMH, EA 3178), Ecole Nationale Supérieure de Céramique Industrielle, 47 à 73 Avenue Albert Thomas, 87065 Limoges cedex, France

Received 8 June 2001; received in revised form 29 November 2001; accepted 8 December 2001

Abstract

Early hydration (0–24 h) of Secar 71, a calcium aluminate cement, has been examined in-situ by ultrasonic testing for pastes prepared at 20 °C (W/C = 0.33, 0.38 or 0.40) and at 5 °C, 40 °C and 60 °C (W/C = 0.33). The ultrasonic measurements consist of following the velocity of the longitudinal ultrasonic wave, V_L (frequency = 1 MHz), transmitted inside the specimen and also the reflection coefficient, R, at the interface between the cement and the container of the paste, which is a polymethylmethacrylate mould. The variations of V_L as a function of setting time can be described by a dissolution-precipitation mechanism. Lastly, the changes in R can be linked with morphological changes occurring inside the cement paste, especially the progressive formation of crystallised hydrates.

Keywords: Calcium aluminate cement; Cement; Hydration; Ultrasonic testing

1. Introduction

Calcium aluminate cements (CACs) are the basis of high performance materials and have found recent applications in sewage networks, hydraulic dams, low-cement castables or the so-called "building industry" in applications such as tile cements and self-levelling screeds.[1] These cements contain CaO and Al_2O_3 as the main oxides which combine to give monocalcium aluminate (CA) as the major active phase in the cement. This phase reacts to give calcium aluminate hydrates (CAH_{10}, C_2AH_8 and C_3AH_6) and also aluminia hydrates (AH_3).

Monitoring the hydration at a young age is interesting for knowing the setting time,[2–5] but also to be able to predict the long term behaviour of these materials. The literature concerns mainly works on Portland based materials and mostly on hard specimens.[6–14] Hydration has been examined by several classical techniques, amongst which we can quote calorimetry, electrical conductivity measurements on dilute systems,[15] thermal analysis, X-ray diffraction, scanning electron microscopy. These characterisations correspond to ex-situ analyses after stopping hydration. Some in-situ techniques such as proton and aluminium nuclear magnetic resonance[16] or synchrotron energy-dispersive diffraction have been employed to monitor the hydration of CA.[11,17] For the two techniques, the experiments have been applied to small quantities of matter.

In the present paper, we wish to discuss another non-destructive technique, namely ultrasonic measurements, for examining the early hydration of a commercial aluminous cement (Secar 71). We have chosen to study an aluminous cement containing either no organic admixtures or no other mineral constituents in order not to modify the hydration mechanisms. Previous results presented on the same material showed how this ultrasonic technique is adapted for following in-situ the stiffening of cement paste[18] and why it gives more information than a simple Vicat test.[19] In the present paper, we examine how ultrasonic measurements relate to existing hydration models. We discuss the ultrasonic behaviour at a young age ($t \leqslant 24$ h) and different temperatures (5, 20, 40 and 60 °C) for a paste where the water-to-cement weight ratio, W/C, is equal to 0.33. At 20 °C, we have also prepared additional lots where W/C = 0.38 and 0.40.

* Corresponding author.
E-mail addresses: t.chotard@ensci.fr (T. Chotard), a.smith@ensci.fr (A. Smith).

0955-2219/02/$ - see front matter
PII: S0955-2219(01)00530-1

2. Experimental

2.1. Preparation of the cement paste

The cement is a commercial aluminous material (Secar 71) whose composition and physical characteristics are given in Table 1. The particle size distribution is given on Fig. 1. It ranges between 0.3 and 100 μm with an average size around 10 μm.

The results presented in this paper refer to one cement manufactured at a given date and stored for a short period. Different lots are prepared with this raw material. Mixing is carried out at different temperatures, namely 5, 20, 40 and 60 °C, according to the normalised procedure N° CEN 196–3. Prior to mixing, the constituents are kept at the mixing temperature for 12 h. Each lot of paste is prepared with a water-to-cement weight ratio (W/C) equal to 0.33. At 20 °C, two additional ratios have been tested, namely W/C = 0.38 and 0.40. Table 2 summarises the different notations used for the pastes. For each lot and each temperature, at least three ultrasonic characterisations have been carried out to check the reproducibility of the data.

After mixing, the paste is poured in a polymethylmethacrylate (PMMA) mould prior to ultrasonic measurements. The removal of air is done under a low pressure ($\cong 10^{-1}$ atm) for 5 min. The quantity of paste is sufficiently large to avoid a significant change in the W/C ratio during air removal. The specimen under test is kept in the PMMA mould for 24 h.

Table 1
Chemical composition, either in nature of cementitous phase or in oxide, for the cement

Chemical composition		Percentage (wt.%)
Cementitous phase	$CaAl_2O_4$ (or CA)	56
	$CaAL_4O_7$ (or CA_2)	38
	$Al_2O_3\alpha$	<6
	$Ca_{12}Al_{14}O_{33}$ (or $C_{12}A_7$)	<1
Oxide	CaO	26.6–29.2 wt.%
	Al_2O_3	69.8–72.2 wt.%

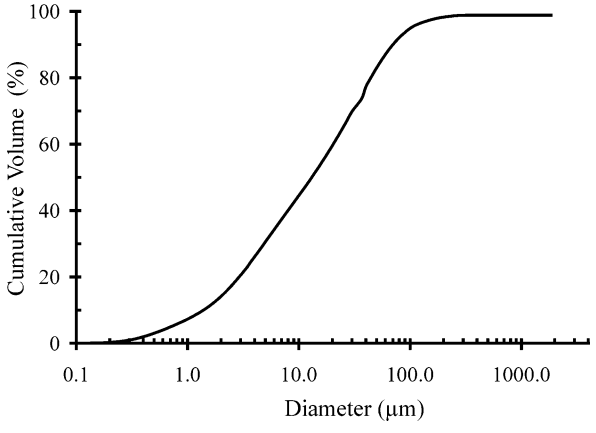

Fig. 1. Particle size distribution for the considered cement.

Table 2
Notations for the mixes prepared at different temperatures, T_{exp}

T_{exp}	5 °C	20 °C			40 °C	60 °C
W/C	0.33	0.33	0.38	0.40	0.33	0.33
Notation	05.033	20.033	20.038	20.040	40.033	60.033

2.2. Characterisation techniques

2.2.1. Ultrasonic measurements

These characterisations are done at 5, 20, 40 and 60 °C. The relative humidity is equal to 95%. This humidity has been chosen according to the normalised procedure CEN 196–1.

Description of the experimental set-up used for ultrasonic measurements is given elsewhere.[19] It consists of setting short pulses of acoustic waves across the specimen under test. These waves are radiated by a source (transducer) with sufficiently low amplitude of vibration for the cement to remain in its viscoelastic or elastic state depending on whether it is a liquid or a solid. Reflection pulse echo technique enables to measure the transit time related to the ultrasonic velocity. In the present case, the experimental set-up is designed to operate in a semi-infinite mode (Fig. 2), which means that the dimensions of the tested sample are very large compared to the ultrasonic wavelength. A transducer sends wideband pulses of longitudinal ultrasonic waves with a central frequency of 1 MHz (Panametric), which propagate into a buffer acting as a delay line. Considering the dimensions of the mould (100×50×10 mm), the average particle size of the cement powder (10 μm) and the typical value of the longitudinal wave velocity of about 3500 m/s measured on 24-h-old cement samples, the value of the central frequency (1 MHz) has been chosen in order to be in accordance with the semi-infinite mode [λ(wavelength)≪dimensions of the mould] and with the homogeneity of the material [λ(wavelength)≫average particle size]. The longitudinal wave velocity has been measured in the 10-mm direction. The proportion of transmitted wave inside the cement-based material depends on the reflection coefficient at the buffer/cement interface. The transit time, t (in seconds), through the cement sample is related to its thickness, e, and the velocity of longitudinal wave, V_L (m s^{-1}), as follows:

$$V_L = \frac{2e}{t} \quad (1)$$

The experimental error on V_L is of the order of 2%. Measurement of t is obtained according to the proce-

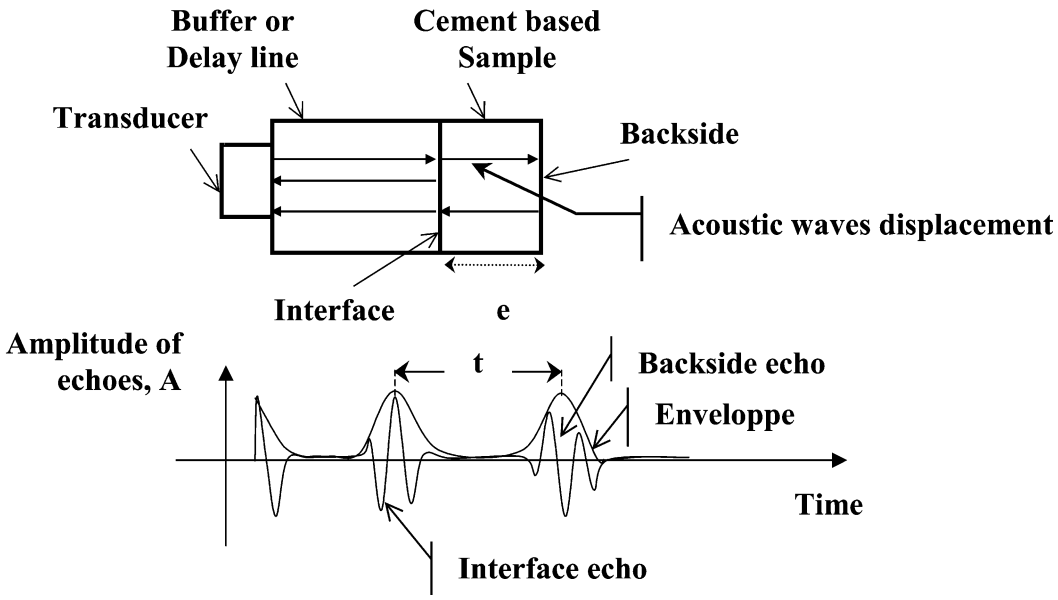

Fig. 2. Experimental setup for ultrasonic measurements.

dure described elsewhere.[20] In addition to the ultrasonic measurements, the temperature of the mixture was recorded during the whole experiment by a T-thermocouple immersed in the sample.

Our experimental set-up also permits to measure the amplitude, A, of the waves reflected at the buffer/cement interface. The corresponding reflection coefficient, R, is related to the acoustic impedance (in kg m^{-2} s^{-1}) of the two materials, namely the cement (Z_{cement}) and the buffer (Z_{buffer}), by the following relation:

$$R = \frac{Z_{cement} - Z_{buffer}}{Z_{cement} + Z_{buffer}} \quad (2)$$

For the present study, the buffer is made of PMMA which has an acoustic impedance close to that of cement when it is in the liquid state. The reflection coefficient approach has already been used by Özturk et al.[10] in order to monitor the setting and hardening of cement-based materials. They used both longitudinal and shear wave reflection factors. This interesting study dealt with Portland mortars containing various additives.

By measuring a reference amplitude, noted A_{ref}, for an echo reflected at the interface between the buffer and a medium with a known acoustic impedance, Z_{ref}, the value of R_{exp} can be deduced:

$$R_{exp} = \frac{A}{A_{ref}} R_{ref} \quad (3)$$

where R_{ref} is the reflection coefficient at the interface between the buffer and the reference medium with its acoustic impedance, Z_{ref}. R_{ref} is given by:

$$R_{ref} = \frac{Z_{buffer} - Z_{ref}}{Z_{buffer} + Z_{ref}} \quad (4)$$

In our case, the reference medium is air where $Z_{ref} \sim 0$ kg m^{-2} s^{-1}. This gives $R_{ref} \sim 1$ and Eq. (3) becomes $R_{exp} \sim A/A_{ref.}$. For a perfect interface between the buffer and the cement, the acoustic impedance is related to the velocity by:

$$Z_{cement} = \rho \, V_L \quad (5)$$

where ρ (in kg m^{-3}) refers to the density of the material. The combination of Eqs. (2) and (5) gives a direct relation between R_{exp} and ρ. Due to the error on A values (maximum $\approx$5–10%), the precision on R_{exp} is of the order of 5–10%.

For experiments at 5 and 20 °C, density variations have been evaluated from measurements of Le Chatelier's shrinkage.[19] From these density values, we can calculate an acoustic impedance using the following relation:

$$Z_{cal} = \rho_{LeChatelier} \times V_L \quad (6)$$

where $\rho_{Le\ chatelier}$ is deduced from hydrostatic measurements. It leads to:

$$R_{cal} = \frac{Z_{cal} - Z_{buffer}}{Z_{cal} + Z_{buffer}} \quad (7)$$

On top of these in-situ characterisations, we have also used other methods for determining the chemical nature of the hydration products. When cement hydration

progresses, the material goes from a paste to a solid state. In order to carry out the ex-situ characterisation of the formed hydration products, specimens of the cement are taken at increasing times. The cement hydration is stopped by a mixture of ethanol and ether in a 1:1 volume ratio.[21] This procedure eliminates the water which is not trapped in hydrates. The resulting product is ground to obtain a powder and characterised by X-ray diffraction (XRD), differential thermal analysis (DTA) and thermogravimetric (TGA) measurements. XRD has been conducted with an INEL CPS 120-Curved Position Sensitive diffractometer. Thermal analysis has been carried out with a DTA-TG coupled RIGAKU thermoflex; each experiment has been done on 96 mg of product under dry nitrogen with a heating ramp of 15 °C/min. The reference material is a calcined alumina from PROLABO. The quantity of bound water, which is trapped in the hydration products, was estimated from weight losses recorded by TG measurements at 1000 °C.

2.3. Background

2.3.1. Ultrasonic measurements for monitoring the hydration of cement pastes at the early age

Previous results on experiments carried out at 20 °C and 95% relative humidity on aluminous paste have shown that ultrasonic measurements, especially V_L and R variations as a function of setting time, enable to follow in-situ the hydration of cement paste.[19] A typical curve of V_L values as a function of setting time is given in Fig. 3. At the beginning of the experiment, when the velocity remains low (close to the longitudinal velocity in water) and fairly constant while the temperature inside the material changes, hydrates are probably formed in low amounts (Fig. 3, region A). The ultrasonic waves travel across a water like medium. This corresponds to the nucleation phase. In a second stage (Fig. 3, region B), V_L increases notably and the weight loss of bound water (measured by TGA) increases simultaneously, which means that the quantity of formed hydrates is growing. The beginning is characterised by Le Chatelier's shrinkage. The grains come in closer contact to each other as hydration proceeds. The experimental and the calculated reflection coefficients are similar to begin with and there is a point in time when $R_{cal} < R_{exp}$ (Fig. 4). This occurs when crystalline hydrates are detected by XRD. This suggests that R_{exp} is not only sensitive to relative density variation but also to modification of the material structure. Lastly, in zone C, V_L and R reach asymptotic values which are characteristic of a set cement.

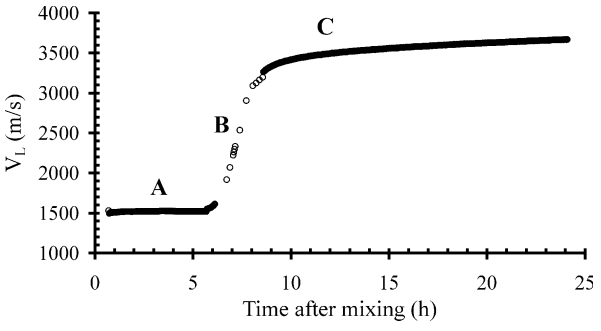

Fig. 3. Typical curve of V_L as a function of time.

2.3.2. Possible description of hydration mechanism in cement paste: dissolution-crystallisation and surface diffusion

The first theory is based on congruent dissolution of anhydrous phases followed by precipitation of hydrates.[22–26] Experiments on dilute systems have been interpreted from this theory. According to this approach, grains of CA dissolve in the form of Ca^{2+} and $Al(OH)_4^-$ ions. Their concentration rapidly reaches sursaturation compared to what is necessary for the formation of hydrates. Therefore, germs of hydrates start to nucleate. After this nucleation, during the so-called "dormant period", the germs grow until they reach a critical size. Thereafter there is a massive precipitation of hydrates which is accompanied by an important heat generation. In reality, even if the germs form very early, i.e. just after mixing the constituents, they cannot be detected immediately by techniques such as X-ray diffraction, thermal analysis or scanning electron microscopy.

The second theory of hydration has been described by Fujii et al.[27] Its particularity is in the fact that nucleation takes place at the surface of anhydrous grains and not in solution. Fujii et al. report the hydration of CA where the water to CA weight ratio (W/C) varies between 0.5 and 5. The hydration was studied in the paste state from 10 to 30 °C. According to these authors, the solution state is maintained almost constant during the induction period while an intrusion-hydrated layer on the CA particles grows. This layer is composed of hydrated CA particles and $Al(OH)_3$ gel. When the layer grows to reach a critical thickness ($\cong$3 nm at 10–20 °C

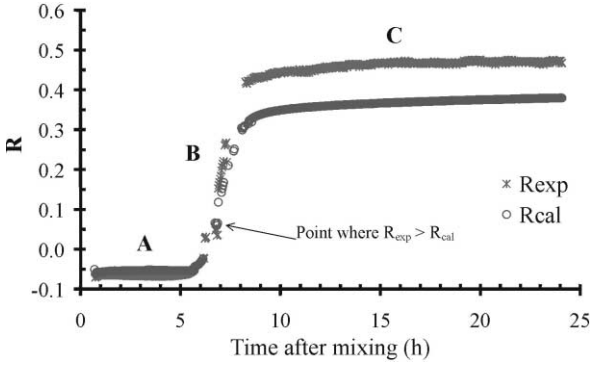

Fig. 4. Variations of R_{exp} and R_{cal} as a function of time for the specimen prepared with W/C = 0.33 at 20 °C (specimen 20.033).

or 12 nm at 30 °C), destruction of the layer occurs due to stress caused by intruded water molecules. Upon destruction of the hydrated layer, nuclei of the hydrous compounds likely to form at a given temperature are generated and at the same time the induction period is terminated. The nucleation occurs on the surface of CA particles.

The third theory is based on more recent work[11,12,17] describing hydration kinetics of CA using synchrotron energy-dispersive diffraction on small quantities of cement paste, typically 2 or 3 g. The results reported concern experiments at temperatures ranging from 60 to 90 °C. Rashid et al.[11,12] show that CA hydration in this temperature range goes through successive steps: a layer of hydrated products forms around the CA grains and progressively hinders the penetration of water thus stopping the reaction between CA and water.

Different kinetics models exist to describe hydration of hydraulic binders and they relate the hydration rate, α (with $0<\alpha<1$), and the time, t (Table 3). Schiller[28–32] has developed a mathematical model based on a dissolution and precipitation mechanism to describe the hydration of plaster. In Eq. (3.1), Table 3), K_1 is the induction time,$(K_2)^{-1}$ is proportional to the growth rate constant and to the number of nuclei of the new hydrated phase, and $(K_3)^{-1}$ is proportional to the dissolution rate constant and to the number of anhydrous particles. Some authors[13] mention the basic Avrami–Erofeew's equation,[33–35] which is also based on a dissolution-precipitation mechanism. This equation makes assumptions about the shape of the nuclei. Avrami–Erofeew's model has been applied to specific cements such as Portland or blast slag cements, but it has never been used in the case of aluminous cements, probably due to the difficulty in describing precisely the shape of the growing phases. Another series of models concerns the diffusion mechanism at the surface of anhydrous grains.[36] These models assume that the solid surface is progressively covered by a layer of hydration products. In Eq. (3.2) which refers to a three-dimensional diffusion model (Table 3), K_D is the diffusion process rate.

3. Results and discussion

Figs. 5 and 6 show the variations of the longitudinal velocity, V_L, and temperature T for the mixture prepared with a W/C ratio equal to 0.33.

Table 3
Kinetic models for describing the hydration of cement based materials

Mechanism	Equation	
Dissolution—precipitation	$t = K_1 + K_2\alpha^{1/3} + K_3\left[1-(1-\alpha)^{1/3}\right]$	(3.1)
Surface diffusion	$t = K_D\left[1-(1-\alpha)^{1/3}\right]$	(3.2)

For each experiment, characteristic parameters have been determined as shown in Fig. 7 and are summarised in Table 4. T_{exp} corresponds to the temperature of experiment. $t^0_{V_L}$ and $t^1_{V_L}$ refer to the times when there is a significant modification of slope for V_L. t^0_T coincides with the beginning of the temperature rise. V_L^{ini} and $V_L^{24\ h}$ are the ultrasonic velocities at the beginning of the

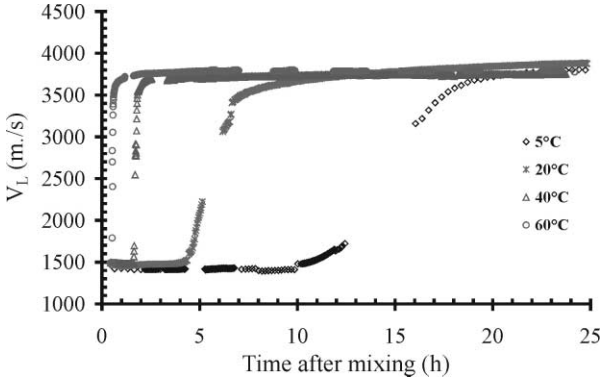

Fig. 5. Variations of V_L as a function of time for the specimens prepared with W/C = 0.33 at different temperatures: (a) 5 °C (specimen 05.033), (b) 20 °C (specimen 20.033), (c) 40 °C (specimen 40.033), (d) 60 °C (specimen 60.033).

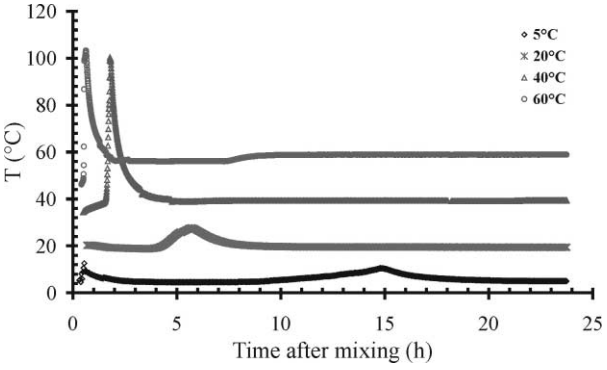

Fig. 6. Variations of the temperature recorded inside the cement as a function of time for the specimens prepared with W/C = 0.33 at different temperatures: (a) 5 °C (specimen 05.033), (b) 20 °C (specimen 20.033), (c) 40 °C (specimen 40.033), (d) 60 °C (specimen 60.033).

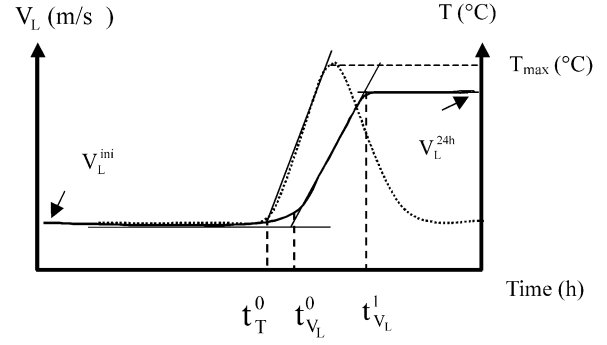

Fig. 7. Characteristic parameters extracted from the V_L and temperature versus time curves.

Table 4
Characteristic parameters deduced from V_L and T variations for the cement pastes

Specimen	05.033	20.033	40.033	60.033
T_{exp} (°C)	5	20	40	60
$t^0_{V_L}$ (h:min)	10:00	4:25	1:35	0:30
$t^1_{V_L}$ (h:min)	18:00	6:47	2:00	0:50
t^0_T (h:min)	9:00	4:00	1:35	0:30
V_L^{ini} (min/s)	1419	1480	1485	1495
$V_L^{24\ h}$ (min/s)	3800	3884	3850	3779
V_L^{water} (min/s)	1397	1425	1465	1479
T_{max} (°C)	10	27	100	103

ultrasonic measurements and at 24h. $V_L^{water}$is the longitudinal velocity which has been measured is distilled water at T_{exp}.

Data in Table 4 show that V_L^{ini} increases with T_{exp}. At the beginning of ultrasonic measurements, the waves propagate in a material which is essentially in the liquid phase. V_L^{ini} is very close to V_L^{water} which suggests that the rheological behaviour of cement is very close to the one of water. We can also notice that t^0_T and $t^0_{V_L}$ decrease when T_{exp} increases. The higher the temperature is, the shorter is the nucleation period or the duration during which V_L remains constant. This result is not quite in accordance with literature data.[15,24,26,37–42] Indeed, several studies about the delay in setting time for aluminous cements and carried out at different temperatures show that the setting time increases when the temperature goes from 5 to 30 °C and decreases when the temperature is greater than 30 °C. Our results are not in accordance with the literature and the explanation is that the cement material which is used nowadays has a slightly different mineral composition compared to the cement sold several years ago.[43]

We can also notice that the difference between t^0_T and $t^0_{V_L}$, on the one hand, and between $t^0_{V_L}$and $t^1_{V_L}$, on the other hand, decreases when T_{exp} increases. The difference between t^0_T and $t^0_{V_L}$ corresponds to the minimum quantity of hydrates to be formed so that V_L can start increasing.[19] The difference between $t^0_{V_L}$and $t^1_{V_L}$is linked with the cement stiffening; this rigidification is faster when the temperature is higher.

Lastly, the comparison between R_{exp} and R_{cal} for measurements done at 5 °C (Fig. 8) and at 20 °C (Fig. 4) show that $R_{exp} > R_{cal}$ when $t > 10$ h at 5 °C and when $t > 5$ h at 20 °C.

3.1. Correlation between the ultrasonic parameters and the physico-chemical characteristics of the cement

Fig. 9 presents on the same diagram the variations of V_L and of the percentage of bound water for the different specimens. For each temperature, the variations of these two sets of experimental points occur simultaneously. For V_L and the percentage of bound water, we

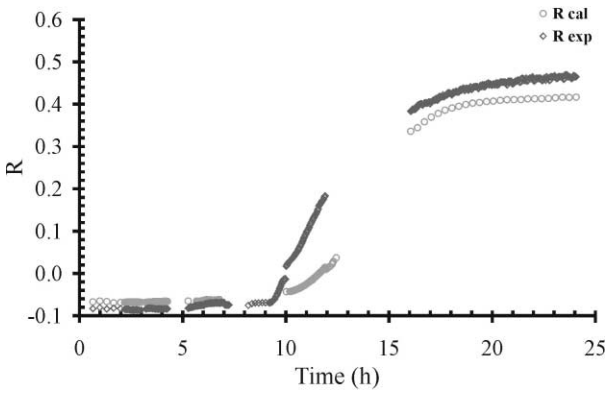

Fig. 8. Variations of R_{exp} and R_{cal} as a function of time for the specimen prepared with W/C = 0.33 at 5 °C (specimen 05.033).

can define a time, $t_{50\%}$. It is the average between the time where V_L and the percentage of bound water have the lowest and the highest values. The $t_{50\%}$ (V_L) and $t_{50\%}$ (bound water) values are very close as reported on Table 5. It means that the ultrasonic velocity is sensitive to massive formation of hydrates. For each temperature, specimens have been analysed at different times by DTA (Fig. 10) and XRD (Fig. 11). Table 6 summarises the information extracted from these two techniques, especially the chemical nature of the hydrates and their form (amorphous or crystalline). In the case of crystalline hydrates and for each temperature, we have determined the width at half-height, $\Delta 2\theta$, for the most intensive peaks (Table 7) at increasing times.

The results show that the chemical nature of the hydrates depends on the temperature. At 5 °C, hydration products are CAH_{10} and AH_3 as analysed by DTA. CAH_{10} is detected in crystalline form 10 h after mixing water and cement. At 20 °C, a mixture of CAH_{10}, C_2AH_8 and AH_3 is formed. At 40 °C, the major hydrated constituents are C_2AH_8 and AH_3. Lastly, at 60 °C, C_3AH_6 progressively becomes the major calcium aluminate hydrate. At 20, 40 or 60 °C, when AH_3 is crystallised, it is in the form of gibbsite. However, as evidenced by DTA, AH_3 can be present at different times and temperatures, but probably in a non crystalline form.

For each temperature, if we compare the time at which crystalline hydrates are detected and the evolution of width at half-height of the diffraction peaks ($\Delta 2\theta$), we can make the following comments:

1. at 5 °C, crystallised CAH_{10} is detected at 10h, which is very close to $t^0_{V_L}$and shortly after t^0_T.

Table 5
$t_{50\%}$ for the different mixtures

Specimen	05.033	20.033	40.033	60.033
t_{50} (Bound water; h:min)	14:25	5:45	1:45	1:30
t_{50} (V_L; h:min)	14:20	5:40	1:50	1:35

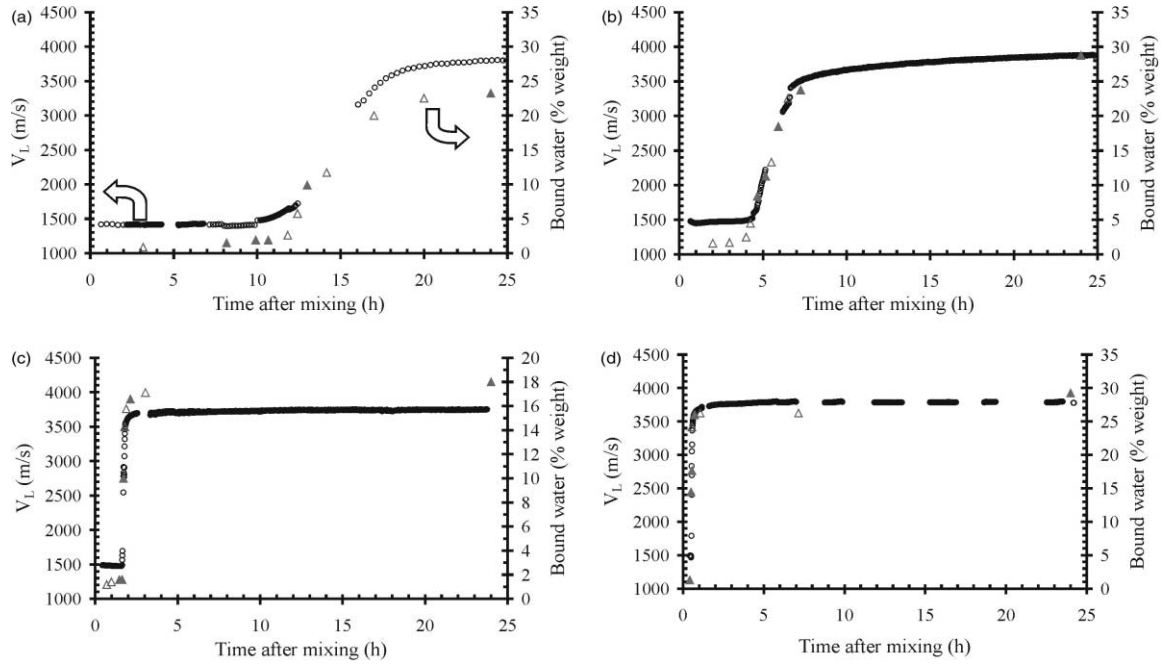

Fig. 9. Variations of V_L and bound water for the different specimens prepared with W/C = 0.33 at different temperatures: (a) 5 °C (specimen 05.033), (b) 20 °C (specimen 20.033), (c) 40 °C (specimen 40.033), (d) 60 °C (specimen 60.033). Symbols: (○) V_L, (△) bound water, (▲) time at which specimens have been analysed ex-situ by TGA and XRD.

Beyond this time, $\Delta 2\theta$ (CAH_{10}) does not change significantly.

2. at 20 °C, crystallised CAH_{10} is beginning to be detected by XRD at a time located between $t^0_{V_L}$ and $t^1_{V_L}$. $\Delta 2\theta$ (CAH_{10}) decreases between 6 h and 7 h 15 min, and it has a constant value till 24 h. With respect to C_2AH_8, it is detected by XRD just after $t^1_{V_L}$ and $\Delta 2\theta$ (C_2AH_8) decreases with time.
3. at 40 °C, crystallised C_2AH_8 appears between $t^0_{V_L} = 1$ h 25 min and $t^1_{V_L} = 2$ h. $\Delta 2\theta$ (C_2AH_8) decreases when the setting time goes from 2 h 10 min and 24 h.
4. at 60 °C, crystallites of C_3AH_6 and AH_3 are detected between $t^0_{V_L} = 0$ h 30 min and $t^1_{V_L} = 0$ h 50 min. In both cases, $\Delta 2\theta$ does not change much with time.

All these results tend to show that the crystallographic changes inside the hydrates are quite important between $t^0_{V_L}$ and $t^1_{V_L}$ and are less marked afterwards. Though the crystallographic characteristics of the hydrates such as crystal size, stoiechiometry or structural arrangement are probably temperature dependent, they do not seem to change drastically once the crystals are formed. Therefore, after $t^1_{V_L}$, we can assume there is little diffusion or changes in stoiechiometry inside the hydrates.

It is also interesting to notice that when crystalline phases are detected at 5 °C, it is also the time when $R_{exp} > R_{cal}$. This crystallisation could be one possible phenomenon responsible for this difference between R_{exp} and R_{cal}. Further investigations are necessary to look more specifically at the mechanical and morphological characteristics of the sample in the vicinity of the interface with the mould.

3.2. Description of hydration mechanism by V_L measurements

In order to correlate the variations of V_L with microstructural changes and eventually a possible hydration mechanism as proposed in Table 3, we have defined the α parameter as follows:

$$\alpha = \frac{V_L - V_{L_0}}{V_{L_1} - V_{L_0}} + \alpha_0 \tag{8}$$

where V_{L_0} (resp. V_{L_1}) represents the ultrasonic velocity at $t^0_{V_L}$ (resp. at $t^1_{V_L}$). At t^0_T, a small quantity of bound water is detected (1.9, 2.5, 1.6 and 1.3% at 5, 20, 40 and 60 °C, respectively). The α value is calculated at different temperatures from V_L-time data. These α parameters are then introduced in Eqs. (3.1) and (3.2) (Table 3). For each temperature, the model which fits best the experimental data points is Schiller's. An example of a good fit between the experimental data and Schiller's model in given in Fig. 12 in the case of 20 °C. Table 8 summarises the K_1, $(K_2)^{-1}$ and $(K_3)^{-1}$ for the different situations. K_1 corresponds to the induction time, or the time beyond which massive formation of hydrates starts. K_1 is close to $t^0_{V_L}$.

First of all, let us examine the variations of $(K_2)^{-1}$ and $(K_3)^{-1}$ at 20 °C but for increasing W/C ratios. $(K_2)^{-1}$

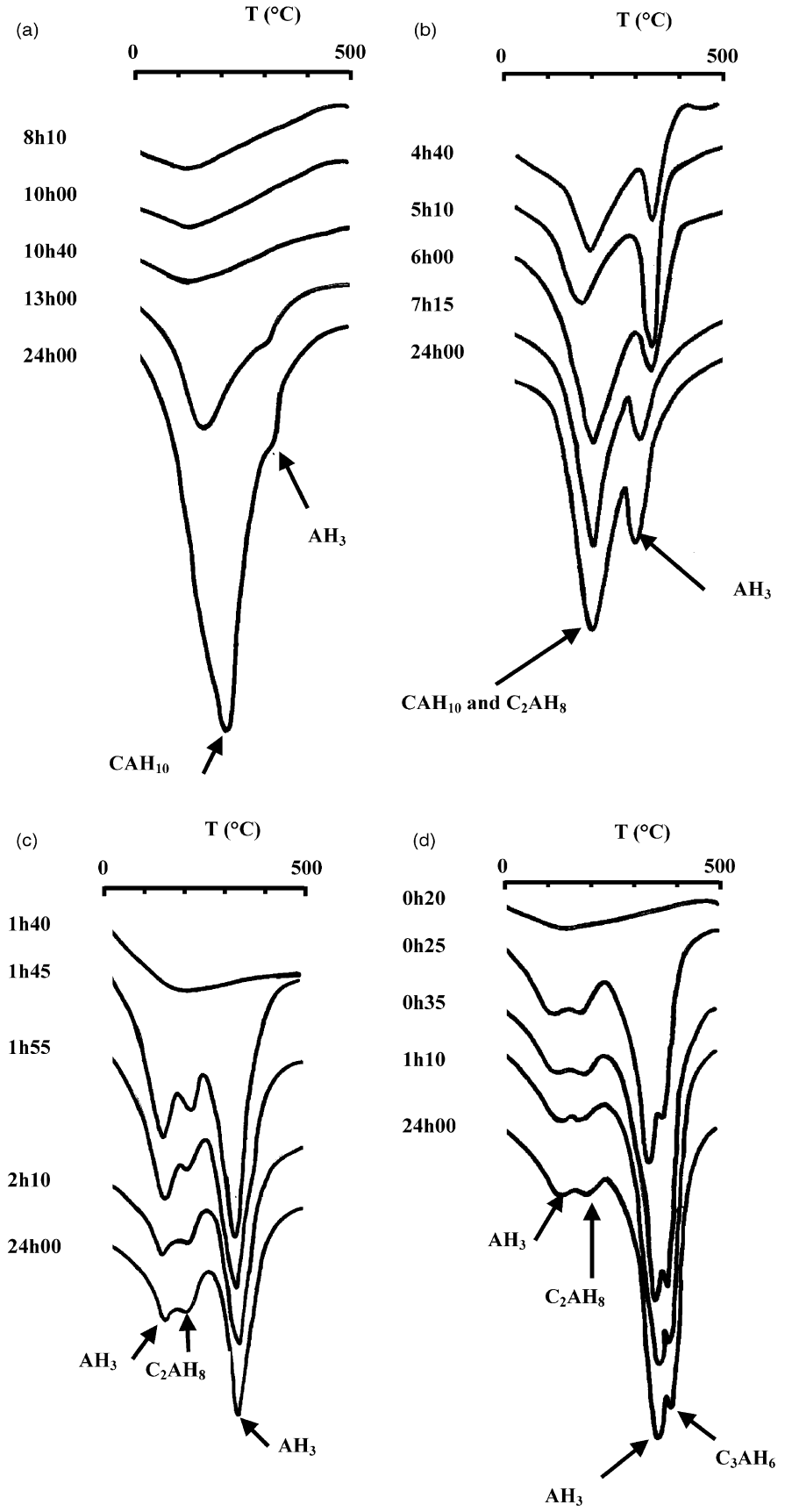

Fig. 10. DTA diagrams for the specimens prepared with W/C = 0.33 at different temperatures: (a) 5 °C (specimen 05.033), (b) 20 °C (specimen 20.033), (c) 40 °C (specimen 40.033), (d) 60 °C (specimen 60.033) for different times.

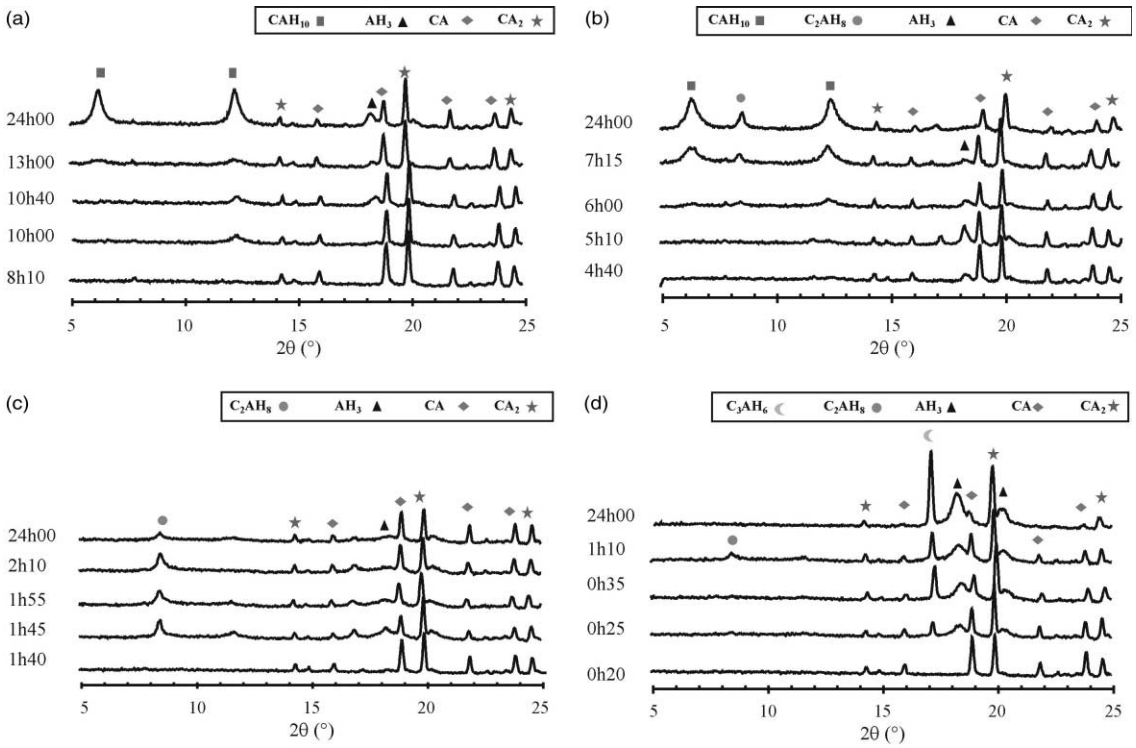

Fig. 11. XRD diagrams for the specimens prepared with W/C = 0.33 at different temperatures: (a) 5 °C (specimen 05.033), (b) 20 °C (specimen 20.033), (c) 40 °C (specimen 40.033), (d) 60 °C (specimen 60.033) for different times.

Table 6
Type of hydrates formed at different temperatures during the first 24 h and detected by DTA or XRD

Specimen	Time (h:min)	DTA	XRD
05.033	8:10	CAH_{10}	–
	10:00	CAH_{10}	CAH_{10}
	10:40	CAH_{10}	CAH_{10}
	13:10	CAH_{10}	CAH_{10}
	24:00	CAH_{10} and AH_3	CAH_{10}
20.033	4:00	CAH_{10}, C_2AH_8 and AH_3	–
	4:40	CAH_{10}, C_2AH_8 and AH_3	–
	5:15	CAH_{10}, C_2AH_8 and AH_3	CAH_{10}
	6:00	CAH_{10}, C_2AH_8 and AH_3	CAH_{10} and C_2AH_8
	24:00	CAH_{10}, C_2AH_8 and AH_3	CAH_{10} and C_2AH_8
40.033	1:40	C_2AH_8 and AH_3	–
	1:45	C_2AH_8 and AH_3	C_2AH_8 and AH_3
	1:55	C_2AH_8 and AH_3	C_2AH_8 and AH_3
	2:10	C_2AH_8 and AH_3	C_2AH_8 and AH_3
	24:00	C_2AH_8 and AH_3	C_2AH_8 and AH_3
60.033	0:20	–	–
	0:25	C_2AH_8, C_3AH_6 and AH_3	C_2AH_8, C_3AH_6 and AH_3
	0:35	C_2AH_8, C_3AH_6 and AH_3	C_2AH_8, C_3AH_6 and AH_3
	1:10	C_2AH_8, C_3AH_6 and AH_3	C_2AH_8, C_3AH_6 and AH_3
	24:00	C_2AH_8, C_3AH_6 and AH_3	C_2AH_8, C_3AH_6 and AH_3

decreases when W/C increases. $(K_3)^{-1}$ is fairly constant for W/C = 0.33 and 0.38, and increases slightly for W/C = 0.4. $(K_3)^{-1}$ is proportional to the number of anhydrous particles and to the dissolution rate constant. Fujii et al.[27] show that $(K_3)^{-1}$ remains constant whatever the W/C ratio is. These authors have studied more dilute systems (W/C = 0.5–5) than in the present case. The small increase of $(K_3)^{-1}$ for W/C = 0.4 cannot be attributed to an increase in the number of cement particles since the cement is more diluted than W/C = 0.33 or

Table 7
Half-height width of diffraction rays at $2\theta = 12.362°$, 8.256°, 17.271° and 18.282° for CAH_{10}, C_2AH_8, C_3AH_6 and AH_3 hydrates, respectively, as a function of time for the specimens prepared with W/C = 0.33 at 5 °C (specimen 05.033), at 20 °C (specimen 20.033), at 40 °C (specimen 40.033) and at 60 °C (specimen 60.033)

	Specimen					
	05.033	20.033		40.033	60.033	
Time (h:min)	$\Delta 2\theta$ (CAH_{10})	$\Delta 2\theta$ (CAH_{10})	$\Delta 2\theta$ (C_2AH_8)	$\Delta 2\theta$ (C_2AH_8)	$\Delta 2\theta$ (C_3AH_6)	$\Delta 2\theta$ (AH_3)
0:25	–			–	0.14	0.50
0:33	–			–	0.17	0.48
1:10	–			–	0.17	0.49
1:45	–			0.31	–	–
1:55	–			0.30	–	–
2:10	–			0.29	–	–
6:00	–	0.63		–	–	–
7:15	–	0.44	0.38	–	–	–
10:00	0.40			–	–	–
10:15	0.39			–	–	–
24:00	0.35	0.43	0.30	0.21	0.16	0.55

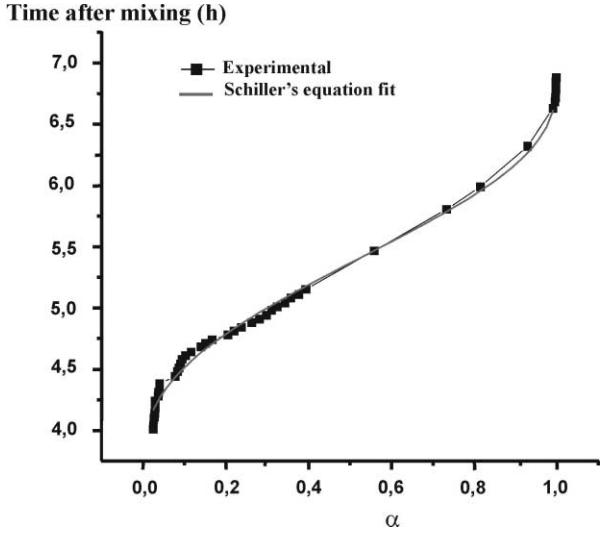

Fig. 12. Comparison between experimental data and Schiller's model for the specimen prepared with W/C = 0.33 at 20 °C (specimen 20.033).

0.38. It can be due to an improved dissolution of the particles since there is a better contact between the cement and the water. Concerning $(K_2)^{-1}$, it is related to the number of nuclei and to their growth rate constant. If the number of nuclei is strictly related to the dissolution of anhydrous particles, we can assume in the present case that this number does not change very much with the W/C ratio and only depends on the temperature. Consequently, the drop in $(K_2)^{-1}$ could be associated with a decrease in the growth rate constant. If hydrates growth is less active, it could account for a lengthening of the $t^1_{V_L} - t^0_{V_L}$ interval, which means a slower rigidification when the W/C ratio increases.

Therefore, these results at 20 °C show that V_L variations as a function of setting time are in favour of a dissolution-precipitation mechanism rather than a diffusion at the surface of anhydrous grains. This is in accordance with results obtained on dilute system (W/C = 10).[26]

Table 8
K_1, $(K_2)^{-1}$ and $(K_3)^{-1}$ values for the different experiments [specimens prepared with W/C = 0.33 at 5 °C (specimen 05.033), at 20 °C (specimen 20.033), at 40 °C (specimen 40.033) and at 60 °C (specimen 60.033)] deduced from Schiller's equation [Eq. (3.1) Table III], and associated correlation coefficient, R^2

Specimen	K_1 (h:min)	$(K_2)^{-1}(h^{-1})$	$(K_3)^{-1}(h^{-1})$	R^2
05.033	9:41	0.206	0.237	0.991
20.033	3:37	0.559	0.662	0.994
20.038	3:55	0.505	0.633	0.995
20.040	4:47	0.360	0.758	0.995
40.033	1:33	5.556	12.50	0.993
60.033	0:28	14.29	50.00	0.979

Let us now look at the variations of $(K_2)^{-1}$ and $(K_3)^{-1}$ at various temperatures and for W/C = 0.33. $(K_2)^{-1}$ and $(K_3)^{-1}$ increase with temperature. If we assume that the number of anhydrous particles is similar in all cases since the W/C ratio is identical, the increase in $(K_3)^{-1}$ can be due to a rise in the dissolution rate constant which corresponds to a thermally activated phenomenon. Concerning $(K_2)^{-1}$, its increase with temperature could be linked to either a larger number of nuclei or to a higher growth rate constant. Evidence for this hypothesis can be deduced from XRD data. $\Delta 2\theta$ (C_2AH_8) measured at 20 °C and 24 h is greater than $\Delta 2\theta$ (C_2AH_8) measured at 40 °C and 24 h (Table 7). If we assume, in a first approximation that $\Delta 2\theta$ is inversely proportional to the crystal size, the size of C_2AH_8 hydrates increases when the temperature goes from 20 to 40 °C. This could be explained by a higher growth rate constant. We can also suppose that the number of nuclei increases with T_{exp}. Studies on solution growth of single oxides have already demonstrated that more nuclei are formed when the temperature rises.

4. Conclusion

These results show that ultrasonic experiments can provide information about the early hydration of CAC. We have shown it is possible to determine precisely the duration of rigidification; it corresponds to the interval where the longitudinal velocity varies significantly. In this respect, ultrasonic measurements could be a useful characterisation for monitoring in-situ cement setting since it gives more information than the classical Vicat test. For the temperatures tested in the present study (5, 20, 40 and 60 °C) and for the chosen W/C ratios (0.33 for each temperature, 0.38 and 0.40 for 20 °C), it seems that the hydration of aluminous cement is a dissolution-precipitation process. The influence on the hydration mechanism of parameters such as particle size distribution, chemical composition, morphology of particles, and crystallographic nature of crystal planes which constitute the surface of the anhydrous cement particles, could give a more precise signature of $(K_2)^{-1}$ and $(K_3)^{-1}$. Lastly, the other ultrasonic parameter, R_{exp}, seems to be linked to morphological changes of hydrates and especially to their crystallisation.

Acknowledgements

The authors wish to thank Dr. H. Fryda, Dr. R. Roesky and Dr. K. Scrivener from Lafarge Aluminates in l'Isle d'Abeau (France) for supplying cement powder.

References

1. Scrivener, K. L., Cabiron, J. L. and Letourneux, R., High-performance concretes from calcium aluminate cements. *Cem. Conc. Res.*, 1999, **29**, 1215–1223.
2. Mayfield, B. and Bettison, M., Ultrasonic pulse testing of high alumina cement concrete. *Concrete, 1974, 36–38*.
3. Cannard, G., Orcel, G. and Prost, J., Le suivi de la prise des ciments par ultrasons. *Bull. Liaison Labo. Ph. et Ch.*, 1990, **168**, 89–95.
4. Sayers, C. M. and Dahlin, A., Propagation of ultrasound through hydrating cement pastes at early times. *Adv. Cem. Bas. Mater.*, 1993, **1**, 12–21.
5. Sayers, C. M. and Grenfell, R. L., Ultrasonic propagation through hydrating cements. *Ultrasonics*, 1993, **31**(3), 147–153.
6. Boumiz, A., Vernet, C. and Cohen-Tenoudji, F., Mechanical properties of cement and mortars at early ages. *Adv. Cem. Bas. Mater.*, 1996, **1**, 94–106.
7. Escalante-Garcia, J. I. and Sharp, J. H., Effect of temperature on the hydration of the main clinker phases in Portland Cements: Part I, neat cements. *Cem. Conc. Res.*, 1998, **28**, 1245–1257.
8. Escalante-Garcia, J. I. and Sharp, J. H., Effect of remperature on the hydration of the main clinker phases in Portland Cements: Part II, blended cements. *Cem. Conc. Res.*, 1998, **28**, 1258–1274.
9. Escalante-Garcia, J. I., Mendoza, G. and Sharp, J. H., Indirect determination of the Ca/Si ratio of the C-S-H gel in Portland Cements. *Cem. Conc. Res.*, 1999, **12**, 1999–2003.
10. Ozturk, T., Rapoport, J., Popovics, J. S. and Shah, S. P., Monitoring the setting and hardening of cement-based materials with ultrasound. *Conc. Sci. Eng.*, 1999, **1**, 83–91.
11. Rashid, S., Barnes, P., Bensted, J. and Turrilas, X., Conversion of calcium aluminate cement hydrates re-examined with synchrotron energy-dispersive diffraction. *J. Mater. Sci. Lett.*, 1994, **13**, 1232–1234.
12. Rashid, S. and Turrillas, X., Hydration kinetics of $CaAl_2O_4$ using synchrotron energy-dispersive diffraction. *Thermochimica Acta*, 1997, **302**, 25–34.
13. Stepisnik, J. and Lukac, M., Measurement of cement hydration by ultrasonics. *Ceram. Bull.*, 1981, **60**(4), 481–483.
14. Nonnet, E., *Étude de la Température Ambiante à 1600 °C par Méthode Ultrasonore, de Réfractaires Monolithiques*. PhD thesis, Université Paris VI, 1999.
15. Capmas, A., Ménétrier-Sorrentino, D., Damidot, D. Effect of temperature on setting time of calcium aluminate cements. In *Calcium Aluminate Cements*, ed. R. J. Mangabhai. E&F. Spon, 1990.
16. Cong, X. and Kirkpatrick, R. J., Hydration of calcium aluminate cements: a solid-State ^{27}Al NMR study. *J. Am. Ceram. Soc.*, 1993, **76**(2), 409–416.
17. Barnes, P., Clark, S. M., Hausermann, D., Henderson, E., Fentiman, C. H., Muhamad, M. N. and Rashid, S., Time-resolved studies of the early hydration of cements using synchrotron energy-dispersive diffraction. *Phase Transitions*, 1992, **39**, 117–128.
18. Chotard, T. J., Gimet-Bréart, N., Smith, A., Fargeot, D., Bonnet, J. P. and Gault, C., Characterisation of calcium aluminate cement hydration at young age by ultrasonic testing. In *Calcium Aluminate Cements*, ed. R. J. Mangabhai and F. P. Glasser. IOM Communications, London, 2001, pp. 155–167.
19. Chotard, T. J., Gimet-Bréart, N., Smith, A., Fargeot, D., Bonnet, J. P. and Gault, C., Application of ultrasonic testing to describe the hydration of calcium aluminate cement at the early age. *Cem. Concr. Res.*, 2001, **31**, 405–412.
20. Cutard, T., Fargeot, D., Gault, C. and Huger, M., Time delay and phase shift measurements for ultrasonic pulses using autocorrelation methods. *J. Appl. Phys.*, 1994, **75**(5), 1909–1913.
21. Bachiorrini, A. and Guilhot, B., Premières echéances de l'hydratation de l'aluminate monocalcique: influence du protocole de stoppage. *Cem. Concr. Res.*, 1982, **12**, 557–567.
22. Barret, P., Ménétrier, D. and Bertrandie, D., Contribution to the study of the kinetic mechanism of aluminous cement setting. I. Latent periods in heterogeneous and homogeneous milieus and the absence of heterogeneous nucleation. *Cem. Concr. Res.*, 1974, **4**, 545–556.
23. Barret, P. and Ménétrier, D., Contribution to the study of the kinetic mechanism of aluminous cement setting: II. Release of the factor responsible for breaking the latent period by the dissolution of a fraction of the initial Cement. *Cem. Concr. Res.*, 1974, **4**, 723–733.
24. Capmas, A. and Ménétrier-Sorrentino, D., The effect of temperature on the hydration of calcium aluminate cement. In *Proceedings of Unitecr'89*, Trostel ed., The American Ceramic Society, Westerville, 1989.
25. Jiang, S. P., Mutin, J. C. and Nonat, A., Studies on mechanisms and physico-chemical parameters at the origin of the cement setting. I. The fundamental processes involved during the cement setting. *Cem. Concr. Res.*, 1995, **25**(4), 779–789.
26. Sorrentino, D., Sorrentino, F., George, M. Mechanisms of hydration of calcium aluminate cements. In: Skalvy, J. (Ed.), Materials Science of Concrete IV. The American Ceramic Society, 1995.
27. Fujii, K., Kondo, W. and Ueno, H., Kinetics of hydration of monocalcium aluminate. *J. Am. Ceram. Soc.*, 1986, **69**(4), 361–364.
28. Schiller, K., Mechanism of re-crystallisation in calcium sulphate hemihydrate plasters. *J. Appl. Chem.*, 1962, **12**, 135–144.
29. Schiller, K., The setting of a slurry. *J. Appl. Chem.*, 1963, **13**, 572–575.

30. Schiller, K., Effects of impurities and additions on the hydration of calcium sulphate plaster slurries. *J. Appl. Chem.*, 1964, **14**, 209–217.
31. Schiller, K., The ionic concentration in the suspending liquid during the hydration of a slurry. *J. Appl. Chem.*, 1965, **15**, 581–584.
32. Schiller, K., The course of hydration: its practical importance and theoretical iterpretation. *J. Appl. Chem. Biotech.*, 1974, **24**, 379–385.
33. Avrami, M., Kinetics of phase change. I. General theory. *J. Chem. Phys.*, 1939, **7**, 1103–1112.
34. Avrami, M., Kinetics of phase change. II. Transformation-time relations for random distribution of nuclei. *J. Chem. Phys.*, 1940, **8**, 212–224.
35. Avrami, M., Granulation, phase change and microstructure. Kinetics of phase change. III. *J. Chem. Phys.*, 1941, **9**, 177–184.
36. Brown, W. E., Dollimore, D. and Galwey, A.K. In *Comprehensive Chemical Kinetics*, ed. C. H. Berford and C. F. H. Tipper. Elsevier Science, Amsterdam, 1980.
37. Bushnell-Watson, S. M. and Sharp, J. H., The effect of temperature upon the setting behaviour of refractory calcium aluminate cements. *Cem. Conc. Res.*, 1986, **16**(6), 875–884.
38. Bushnell-Watson, S. M. and Sharp, J. H., On the cause of anomalous setting behaviour with respect to temperature of calcium aluminate cements. *Cem. Conc. Res.*, 1990, **20**(1), 677–686.
39. Bushnell-Watson, S. M. and Sharp, J. H., Further studies of the effect of temperature upon the setting behaviour of refractory calcium aluminate cements. *Cem. Conc. Res.*, 1990, **20**(4), 623–635.
40. Edmonds, R. N. and Majumdar, A. J., The hydration of monocalcium aluminate at different temperatures. *Cem. Conc. Res.*, 1988, **18**(2), 311–320.
41. Edmonds, R. N. and Majumdar, A. J., The hydration of $12CaO{\cdot}7Al_2O_3$ at different temperatures. *Cem. Conc. Res.*, 1988, **18**(3), 473–478.
42. Edmonds, R. N. and Majumdar, A. J., The hydration of Secar 71 aluminous cement at different temperatures. *Cem. Conc. Res.*, 1989, **19**(2), 289–294.
43. Lafarge, private communication.